Journal of Alloys and Compounds 507 (2010) 33–37

Contents lists available at ScienceDirect

Journal of Alloys and Compounds

journal homepage: www.elsevier.com/locate/jallcom

# First principles calculations of electronic and optical properties of Mo-doped rutile $TiO_2$

Xiaohui Yu[a,1], Changsheng Li[a,*], Yun Ling[a,b], Ting-Ao Tang[b], Qiong Wu[a], Junjie Kong[c]

[a] School of Material Science and Engineering, Jiangsu University, Zhenjiang, Jiangsu 212013, China
[b] Department of Microelectronics, Fudan University, Shanghai 200433, China
[c] Suzhou Institute of Nano-tech and Nano-bionics, CAS, Suzhou, Jiangsu 215125, China

ARTICLE INFO

*Article history:*
Received 30 April 2010
Received in revised form 6 July 2010
Accepted 27 July 2010
Available online 5 August 2010

*Keywords:*
Rutile $TiO_2$
Mo-doped
First principles
Electronic structures and optical properties
Computer simulation

ABSTRACT

Based on the density functional pseudopotential method, the electronic structures and the optical properties for Mo-doped rutile $TiO_2$ are comparatively investigated in detail. Mo substitution of the Ti sites induces effective reduction of the band gap of $TiO_2$, and the band gap being continuously reduced when increasing Mo doping level. For the pure $TiO_2$, the Fermi level locates at the valence band maximum, while it shifts to the conduction band and exhibits metal-like characteristic after Mo atoms are introduced into the $TiO_2$ supercell. The calculated optical properties indicate that the optical energy gap is increased after Mo doping. More importantly, absorption in the visible-light region is found, which originates from the intraband transition of the Mo 4d bands and the conduction bands. These calculations provide electronic structure evidence that, the Mo-doped rutile $TiO_2$ system could be a potential candidate for photoelectrochemical application due to the increase in its photocatalytic activity.



## 1. Introduction

Up to now, photo-catalysis by titanium dioxide ($TiO_2$) has been investigated extensively for several decades, because it showed several advantages of stability, nontoxicity, and low cost [1]. However, as a serious disadvantage, it needs ultraviolet (UV) radiation to excite the electrons from valence band (VB) to conduction band (CB) because of its wide band gap [2]. Then, to make $TiO_2$ sensitive to a wider range of the solar spectrum, the band gap needs to be narrowed.

In recent years, impurity doping has been widely performed by chemical synthesis and other methods in order to improve photoactivity [3–12]. Theoretical investigations have also been carried out to study the band structures of $TiO_2$ phases including anatase [13–15] and rutile [16–20]. Mo, as a transition metal, has been used to dope $TiO_2$ for photocatalytic applications, showing the effects to make the materials catalytically active under visible light [21–26]. Such investigation has been mainly on the enhancement of the photocatalytic activity, with anatase being the focus of interest. As is well recognized, the rutile phase (3.0 eV, $\lambda \sim 400$ nm) [27] which is the stable form of $TiO_2$, exhibits a direct band structure, while the metastable anatase phase is indirect in nature. The ionic radius of $Mo^{4+}$ is equal to that of $Ti^{4+}$, and values for the first 4 ionization potentials of Mo and Ti are close to each other. $MoO_2$ has a distorted structure of rutile with $c/a = 0.574$, compared to a value of 0.644 for $TiO_2$ rutile, and with pairwise Mo–Mo bonds; bond lengths between Mo in the chains of edge-sharing octahedra alternate between 251 and 311 pm, compared to a constant value of 296 pm between Ti in rutile [28,29]. Thus, rutile $TiO_2$ should be easily doped with $Mo^{4+}$, and at high doping levels the material should exhibit a semiconductor to metal transition. Although little has been done to quantify whether effective red-shift has been caused by Mo doping of rutile $TiO_2$, and no effort has been made for a theoretical characterization of the Mo effects on its electronic and optical properties.

In this theoretical attempt, the aim of work is to study the electronic and optical properties of $TiO_2$ doping with the 4d transition metal Mo. Using the density functional method, to find a probable explanation for the electronic properties of Mo-doped rutile $TiO_2$, and some fundamental information which is similar to the experiments [23,26]. The results suggest that it is important to introduce Mo, which achieve significant red-shift in band gap. Finally, some important optical characteristics that have not been well studied before are analyzed and summed up for the technological applications of this dopant.

* Corresponding author. Tel.: +86 511 88790268; fax: +86 511 88790268.
*E-mail address:* lichangsheng@ujs.edu.cn (C. Li).
[1] Xiaohui Yu was born in Liaoning province. She is a Ph.D. student.

0925-8388/$ – see front matter © 2010 Elsevier B.V. All rights reserved.
doi:10.1016/j.jallcom.2010.07.195

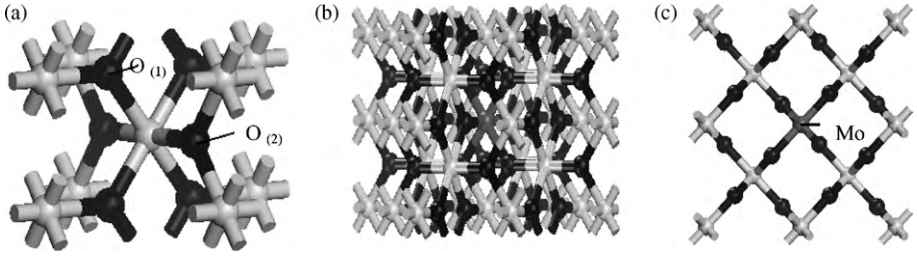


**Fig. 1.** Crystal models: (a) pure rutile $TiO_2$ with each Ti atom (white) bonded to four nearest neighbor O atoms, $O_{(1)}$, and two second nearest neighbor O atoms (black), $O_{(2)}$; (b) $2 \times 2 \times 2$ supercell with a Ti atom being substituted by Mo atom (gray); (c) $2 \times 2 \times 1$ supercell with a Ti atom substituted by Mo atom.

## 2. Calculation models and method

The present quantum-mechanical calculations are performed based on the density functional theory (DFT) and pseudopotential methods, which are implemented in the first principles calculation program CASTEP code [30]. Electronic exchange-correlation energy is treated under generalized gradient approximation (GGA) with the Perdew, Burke, and Ernzerhof (PBE) [31]. The Vanderbilt ultrasoft pseudopotential [32] was used with the cutoff energy of 370 eV, smearing was used with 0.5 eV and a Monkhorst–Pack grid [33] with k-point for irreducible Brillouin zone sampling.

For the geometry optimization of pure rutile and doped rutile $TiO_2$, as shown in Fig. 1, were used $3 \times 3 \times 4$ k-point grids for the $2 \times 2 \times 2$ supercell, and $3 \times 3 \times 8$ k-point grids for the $2 \times 2 \times 1$ supercell doped $TiO_2$ (or pure $TiO_2$). Fine k-point sets $3 \times 4 \times 4$ and $3 \times 5 \times 4$ were employed for calculating the electronic properties of doped rutile $TiO_2$. Test calculations show that using more k-points does not lead to evident changes in the energetic convergence and electronic band structures. Then the electronic structures and optical properties are calculated on the basis of the optimized supercells. In the geometry optimizations, the energetic convergence threshold for self-consistent field (SCF) is $10^{-5}$ eV/atom; atomic relaxation is carried out until all components of the residual forces are less than 0.01 eV/Å, and the maximum ionic displacement was within 0.001 Å. It is worth pointing out that the scheme in Fig. 1, with substitutional Mo at the body-centered (or the base-centered) Ti site in a supercell, helps reduce the distortion of the tetragonal lattice through full structural relaxation. Test calculations reveal ignorable effect due to the artificial interaction between images.

From the viewpoint of quantum mechanics, the photon absorption or emission have caused transition between occupied and unoccupied states, and excitation spectra can be considered as a joint DOS between the valence band and conduction band. Within the linear response, the macro-optical response function of solid usually can be described by the dielectric function. The imaginary part of the dielectric function, $\varepsilon_2(\omega)$, can be written as follows:

$$\varepsilon_2(q \to O_{\hat{u}}, h\omega) = \frac{2\pi e^2}{\Omega \varepsilon_0} \sum_{k,v,c} \left| \left\langle \psi_k^c \left| u \cdot r \right| \psi_k^v \right\rangle \right|^2 \delta(E_k^c - E_k^v - E) \qquad (1)$$

where $u$ is the vector defining the polarization of the incident electric field; $k$ is the reciprocal lattice vector; the superscripts c and v represent the conduction band and valence band, respectively; $E_k^c$ and $E_k^v$ represent intrinsic energy level of conduction band and valence band, respectively; and $\omega$ is the frequency of incident photon. Since the dielectric function shows a causal response, the real part ($\varepsilon_1(\omega)$) of the dielectric function can be obtained from with $\varepsilon_2(\omega)$ the Kramers–Kronig relations. Then the other optical spectra, such as absorption coefficient ($I(\omega)$), reflectivity ($R(\omega)$), refractivity index ($N(\omega)$), and energy loss ($L(\omega)$) can be gained by $\varepsilon_1(\omega)$ and $\varepsilon_2(\omega)$:

$$I(\omega) = \sqrt{2}\omega \left[ \sqrt{\varepsilon_1^2(\omega) + \varepsilon_2^2(\omega)} - \varepsilon_1(\omega) \right]^{1/2} \qquad (2)$$

$$R(\omega) = \left| \frac{\sqrt{\varepsilon_1(\omega) + j\varepsilon_2(\omega)} - 1}{\sqrt{\varepsilon_1(\omega) + j\varepsilon_2(\omega)} + 1} \right|^2 \qquad (3)$$

$$N(\omega) = \frac{\left[ \sqrt{{\varepsilon_1}^2(\omega) + {\varepsilon_2}^2(\omega)} + \varepsilon_1(\omega) \right]^{1/2}}{\sqrt{2}} \qquad (4)$$

$$L(\omega) = \frac{\varepsilon(\omega)}{{\varepsilon_1}^2(\omega) + {\varepsilon_2}^2(\omega)} \qquad (5)$$

## 3. Results and discussion

### 3.1. Optimized structures

The optimized lattice constants are $a = 4.618$ Å and $c = 2.962$ Å for pure $TiO_2$, as is shown in Fig. 1a, which are in good agreement with the experimental values ($a = 4.594$ Å, $c = 2.959$ Å) [34]. The structure parameter of rutile, $u$, is 0.305. Each Ti atom is bonded to four nearest and two second nearest oxygen neighbors. The Mo-doped structures were constructed by using the 48-atom $2 \times 2 \times 2$, and the 24-atom $2 \times 2 \times 1$ supercells with one Ti atom replaced by one Mo atom, those supercells are shown in Fig. 1b and c. Such supercell structures were fully relaxed, and the lattice parameters of the optimized supercells are summarized in Table 1.

**Table 1**
Calculated lattice constants for pure and Mo-doped rutile supercells.

| Structural model | $a$ (Å) | $c$ (Å) | $c/a$ | Ti–O (Å) | Mo–O (Å) | Ti–T (Å) | Ti–Mo (Å) | O–O (Å) | $OTi_3$ or $OTi_2Mo$ |
|---|---|---|---|---|---|---|---|---|---|
| Pure | 4.678 | 2.962 | 0.641 | 1.959<br>2.001 | –<br>– | 3.062<br>2.962<br>4.618 | – | 2.801<br>2.562<br>2.962 | 98.344<br>130.828 |
| 48-doped | 4.683 | 2.967 | 0.634 | 1.963<br>2.016 | 1.979<br>1.990 | 3.616<br>2.970<br>4.684 | 3.664<br>2.971<br>4.706 | 2.763<br>2.655<br>2.958 | 96.461<br>131.750<br>131.188 |
| 24-doped | 4.686 | 2.969 | 0.633 | 1.968<br>2.023 | 1.973<br>1.996 | 3.619<br>2.970<br>4.686 | 3.627<br>2.969<br>4.687 | 2.821<br>2.610<br>2.969 | 98.039<br>130.982<br>130.979 |

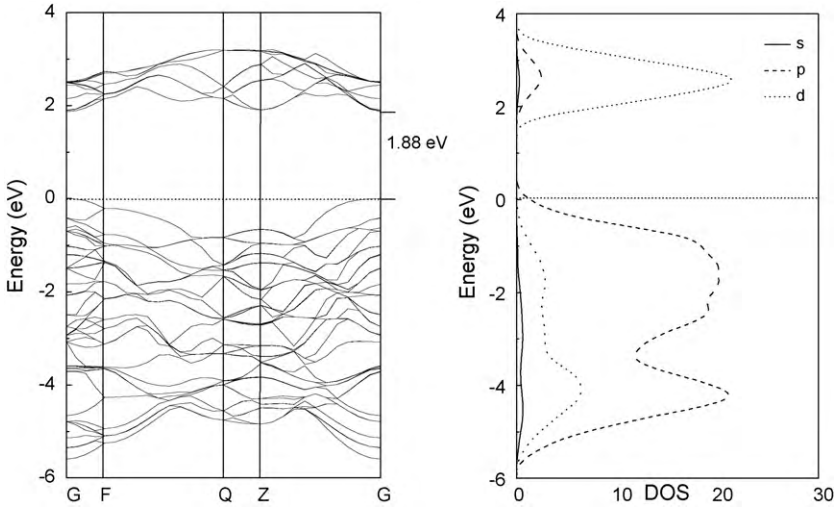


**Fig. 2.** Band structure and DOS for pure rutile $TiO_2$. DOS shows that the top of the valence band is dominated by the oxygen 2p states and the bottom of the conduction band is dictated by the titanium 3d states. The Fermi level is set to 0.

According to the data summarized in Table 1, as the concentration of Mo increasing, the lattice parameters of Mo-doped $TiO_2$ excepts a slight variation and a small elongation along the *c*-axis, which is similar to the experiment [26]. Comparing to the $TiO_2$ rutile phase, the Mo–O bond lengths in the supercells are considerably longer than $Ti–O_{(1)}$ and slight shorter than $Ti–O_{(2)}$. The distortions will be useful to the substitution of Mo for Ti in the $TiO_2$ rutile phase.

### 3.2. Electronic structures

The band structure and density of states (DOS) near the Fermi energy of the pure rutile $TiO_2$ are presented in Fig. 2a and b. It can be seen from Fig. 2a that the valence band maximum and the conduction band minimum locate at the same G point, indicating that the lowest band gap transition in $TiO_2$ rutile is direct, in conformity with the literature [35]. Compared with the experimental value of 3.0 eV, the calculated band gap is underestimated to be 1.88 eV, which is attributed to the well-known intrinsic factor of DFT. It can be seen from the DOS in Fig. 2b that the valence band originates mainly from the O 2p states. In addition, the lowest conduction band is dominated by Ti 3d states. These characteristics are consistent with the previous calculations presented by Stashans et al. [36].

To investigate the doping effect of Mo on the electronic structure, the band structure and DOS are calculated for replacing one Ti site with a Mo atom in the $2 \times 2 \times 2$ (48 atoms) and $2 \times 2 \times 1$ (24 atoms) supercells of rutile, which leads to different levels of doping with Mo accounting for 2.08 and 4.17 at.%, as shown in Figs. 3a and b and 4a and b, respectively. The electron configuration of $Mo^{4+}$ is [Kr] $4d^2$ $5s^0$, and the substructure of the Mo impurity band, as seen for 4 at.% doping in Fig. 4, corresponds to that of the $^3F$ and $^3P$ triplett electronic terms, the first of them splitted in an octahedral ligand field. From the varying degree of overlap of calculated Mo 4d with Ti 3d DOS in Figs. 3 and 4, it could be concluded: for 2 at.% doping the Mo impurity band overlaps fully with the Ti conduction band while for 4 at.% the lowest Mo level is a donor band with localized electrons. Compared with the undoped $TiO_2$, the remarkable feature in energy band for Mo-doped $TiO_2$ is that the Fermi level shifts upward into the conduction band, which indicates that the material is n-type metallic, whereas the incorporation of C on oxygen lattice site will bring different results [37]. At a moderate doping level, e.g., ~6 at.% of the Ti sites in the $2 \times 2 \times 2$ supercell (48 atoms), the O 2p states are the most dominant in the

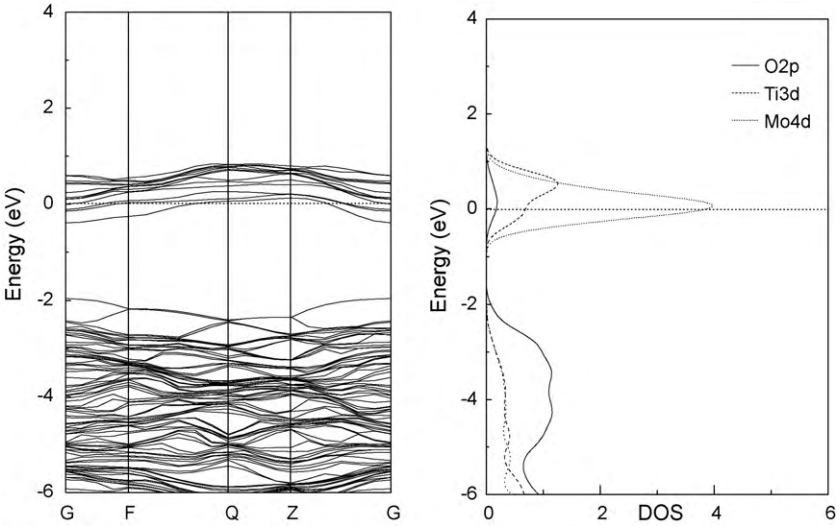


**Fig. 3.** (a) Band structure and (b) DOS for one Mo doping rutile $TiO_2$ using the 48-atom $2 \times 2 \times 2$ supercell. The Fermi level is set to 0.

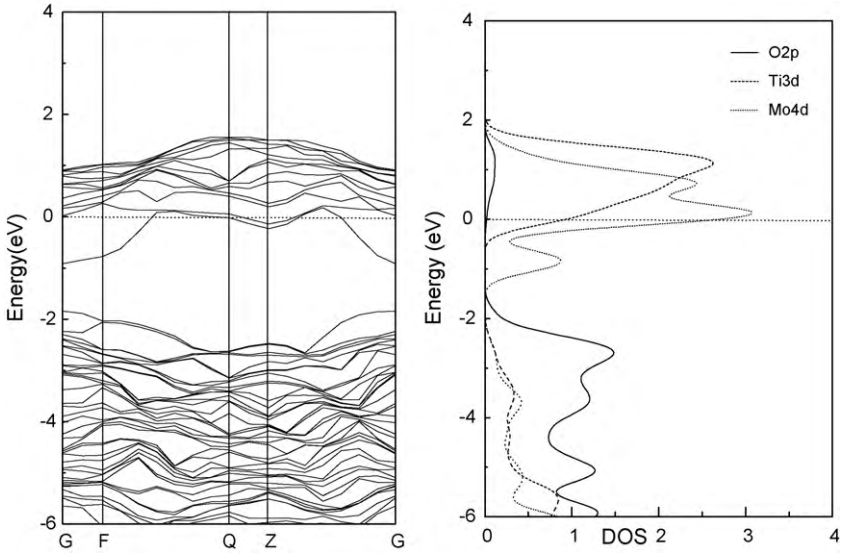


**Fig. 4.** (a) Band structure and (b) DOS for one Mo doping rutile $TiO_2$ using the 24-atom $2 \times 2 \times 1$ supercell. The Fermi level is set to 0.

energy range between −8.1 and −1.6 eV, and the Ti 3d states located mainly in the energy range between −8 and −2 eV and −0.89 and 1.37 eV in Fig. 3b. The impurity bands of Mo 4d states lie just across the Fermi energy, which is partially occupied with a bandwidth of 3.43 eV in Fig. 4b, which is similar to the calculations presented by Murugan et al. [38], the defect levels significantly concentrated in the conduction band. In this situation, the electronic intraband transition form the occupied bands to the unoccupied ones would occur under irradiation, which may induce intense absorption in the long wavelength visible region. On the other hand, the energy difference between valence band maximum and the Fermi level is about 1.96 eV (one Mo in $2 \times 2 \times 2$ supercell), which is larger than the band gap of pure $TiO_2$ (1.88 eV here). As a result, the transition of an electron from valence band to unoccupied states will need more energy in Mo-doped $TiO_2$, and shift to the high-energy region compared with pure $TiO_2$.

### 3.3. Optical properties

Fig. 5 shows the imaginary part of the dielectric function, which is the pandect of the optical properties for the $TiO_2$ systems. For pure $TiO_2$, the major peaks located at 3.43 and 5.8 eV corresponding to two distinct maxima around 300–400 and 200–220 nm in optical absorption spectra respectively. The peak at 3.43 eV originates from the electronic transition between the O 2p states in the upper valence band and the Ti 3d states in the conduction band (Fig. 2). The weak peak at 5.8 eV may be due to the transition between Ti 3d and O 2p states in the valence band. For Mo-doped $TiO_2$ (48 atoms), three main peaks exist at 0.32, 3.39 and 5.78 eV. The peak at around 3.39 eV originates mainly from the transition between Ti 3d and O 2p states (Figs. 3 and 4). The peak in the low region (0.32 eV) comes from the electronic intraband transition of impurity Mo 4d states and Ti 3d states in the conduction band, where the shift of the position corresponds to the localized degree of the impurity band. It can also be seen from Fig. 5 that the line shape is almost the same for the doped and undoped $TiO_2$ systems in the high-energy range. These properties indicate that the different configurations of Mo dopant affect mainly the optical properties in the low energy range.

Because the calculated band gap of pure $TiO_2$ (1.88 eV) is smaller than the experimental value (3.0 eV), the scissor approximation with the value of 1.12 eV is used for the calculated absorption edge to fit the experimental value. Fig. 6 presents the absorption spectrum of the $TiO_2$ systems (doped and undoped $TiO_2$). It can be seen that the absorption region is quite wide, and the main absorption part still locates at the UV region. Comparing with pure $TiO_2$, additional absorption is observed below the absorption edge in the visible region for Mo-doped systems, which is due to the intraband transition of the Mo 4d impurity band and Ti 3d states in the conduction band. Since the Mo doping would become a very important factor influencing the photocatalytic activity of $TiO_2$ due to the intensive visible light absorption, which would also make $TiO_2$ a potential candidate for photoelectrochemical application.

The reflectivity, refractivity index, and loss function of the pure and Mo-doped $TiO_2$ systems in the energy range of ~0–20 eV, as shown in Fig. 7. For the Mo doping systems, the low energy range (<3.7 eV) is characterized by small reflectivity and appreciable refractivity. The ~3.7–6.9 eV range is characterized by strong

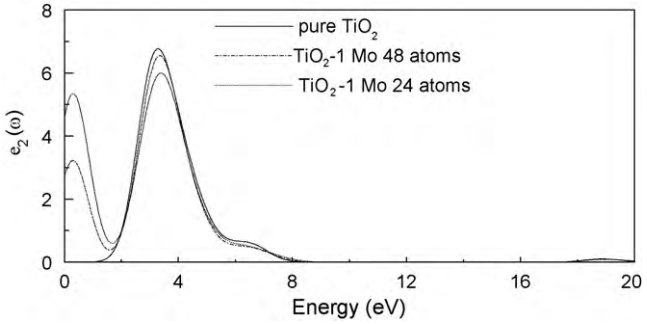


**Fig. 5.** Imaginary part of the dielectric function of Mo-doped and pure $TiO_2$.

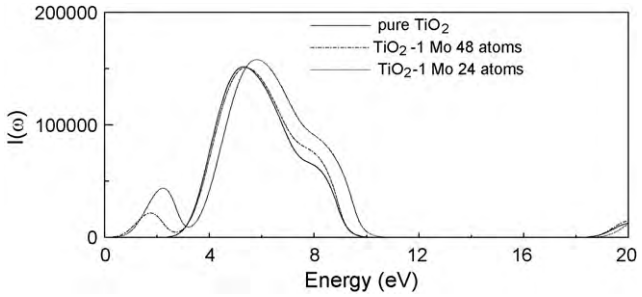


**Fig. 6.** The absorption coefficient spectrum of Mo-doped and pure $TiO_2$.

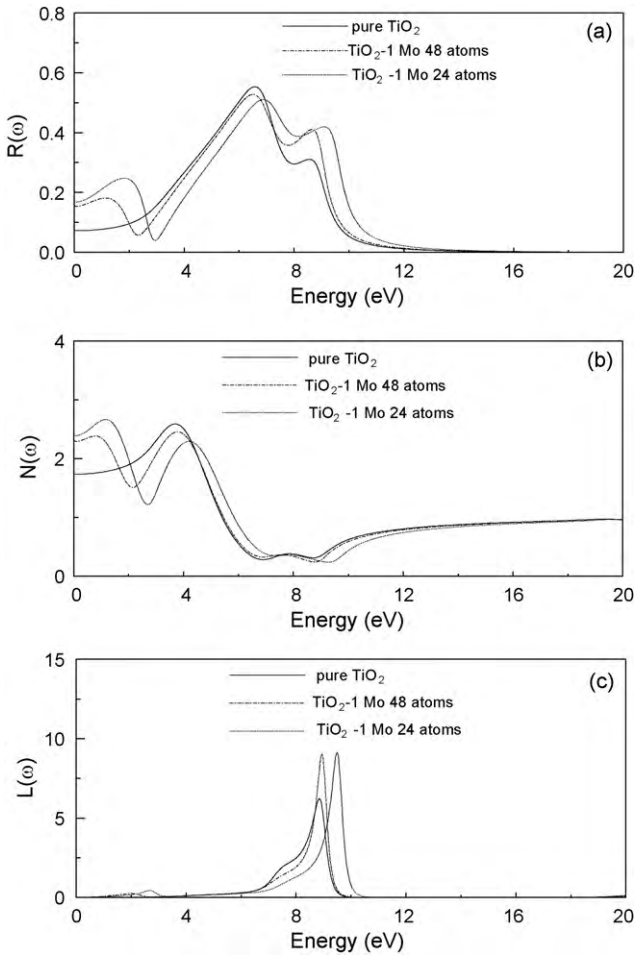


**Fig. 7.** The reflectivity, refractivity index, and energy-loss functions of Mo-doped and pure $TiO_2$ systems.

reflectivity, whereas the refractivity undergoes a change from the strongest to the second weakest. At the range of 3.8–14.6 eV, the reflectivity and refractivity show an opposite trend. The loss function describes the energy loss of the electrons traversing the material. In addition, the peaks of loss function also correspond to the trailing edges in the reflection spectrum [39]. Taking one Mo-doped $TiO_2$ system as an example, the reflectivity reduces abruptly at about 2.1 and 8.9 eV, which corresponds to the peaks of the loss-function spectrum.

## 4. Conclusion

In conclusion, based on the density functional pseudopotential method, the electronic structures and the optical properties of Mo-doped rutile $TiO_2$ are investigated and compared with that of pure $TiO_2$. The electronic structures show that Mo doping $TiO_2$ systems exhibit n-type metallic characteristics. For pure $TiO_2$, the Fermi level is located at the valence band maximum, whereas it shifts to the conduction band and exhibits metal-like characteristics after Mo doping. The calculated optical properties indicate that the optical energy gap is increased after Mo doping. More importantly, a strong absorption in the visible-light region is found, which originates from the intraband transition of the Mo 4d bands and the conduction band. These calculations provide electronic structure evidence that, the Mo doping $TiO_2$ system could be a potential candidate for photoelectrochemical application due to the increase in photocatalytic activity.

## References

[1] O. Legrini, E. Oliveros, A.M. Braun, Chem. Rev. 2 (1993) 671.
[2] J.K. Burdett, et al., J. Am. Chem. Soc. 109 (1987) 3639.
[3] H. Yamashita, Y. Ichihashi, M. Takeuchi, S. Kishiguchi, M. Anpo, J. Synchrotron Rad. 6 (1999) 451.
[4] R. Asahi, T. Morikawa, T. Ohwaki, K. Aoki, Y. Taga, Science 293 (2001) 269.
[5] C. Di Valentin, G. Pacchioni, A. Selloni, S. Livraghi, E. Giamello, J. Phys. Chem. B 109 (2005) 11414–11419.
[6] K. Yang, Y. Dai, B.B. Huang, J. Phys. Chem. C 111 (2007) 12086–12090.
[7] C. Burda, Y. Lou, X. Chen, A.C. Samia, J. Stout, J.L. Gole, Nano Lett. 3 (2003) 1049–1051.
[8] X. Chen, C. Burda, J. Am. Chem. Soc. 130 (2008) 5018–5019.
[9] H. Ozaki, S. Iwamoto, M. Inoue, Catal. Lett. 113 (2007) 95–98.
[10] K. Yang, Y. Dai, B.B. Huang, Chem. Phys. Lett. 456 (2008) 71–75.
[11] T. Umebayashi, T. Yamaki, H. Itoh, K. Asai, Appl. Phys. Lett. 81 (2002) 454–456.
[12] J. Li, H.C. Zeng, J. Am. Chem. Soc. 129 (2007) 15839–15847.
[13] C. Di Valentin, E. Finazzi, G. Pacchioni, A. Selloni, S. Livraghi, C. Maria, Paganini, E. Giamello, Chem. Phys. 339 (2007) 44.
[14] Labat Frédéric, Baranek Philippe, Domain Christophe, Minot Christian, Adamo Carlo, J. Chem. Phys. 126 (2007) 154703.
[15] Lan Mi, Peng Xu, Hong Shen, Pei-Nan Wang, Weidian Shen, Appl. Phys. Lett. 90 (2007) 171909.
[16] C. Wilson Nicholas, E. Grey Ian, P. Russo Salvy, J. Phys. Chem. C 111 (2007) 10915.
[17] M.M. Islam, T. Bredow, A. Gerson 1, Phys. Rev. B 76 (2007) 045217.
[18] C. Lee, P. Ghosez, X. Gonze, Phys. Rev. B 50 (1994) 13379.
[19] Eunae Cho, Seungwu Han, Hyo-Shin Ahn, Kwang-Ryeol Lee, Keun Kim Seong, Seong Hwang Cheol, Phys. Rev. B 73 (2006) 193202.
[20] Kesong Yang, Ying Dai, Baibiao Huang, J. Phys. Chem. C 111 (2007) 18985.
[21] A. Furerte, D.M. Hernandez-Alonso, A.J. Maira, A. Martinez-Arias, M. Fernandez-Garcia, J.C. Conesa, J.J. Soria, Chem. Commun. 24 (2001) 2718.
[22] M.S. Jeon, W.S. Yoon, Joo Hyunku, T.K. Lee, H.J. Lee, Appl. Surf. Sci. 165 (2000) 209.
[23] Ying Yang, Xin-jun Li, Jun-tao Chen, Wang. Liang-yan, J. Photochem. Photobiol. A: Chem. 163 (2004) 517–522.
[24] Hyun You Kim, Hyuck Mo Lee, R.G.S. Pala, V. Shapovalov, H. Metiu, J. Phys. Chem. C 112 (2008) 12398–12408.
[25] Y.Q. Gai, J.B. Li, S.S. Li, et al., Phys. Rev. Lett. 102 (2009) 036402.
[26] L.G. Devi, B.N. Murthy, Catal. Lett. 125 (2008) 320–330.
[27] H. Tang, F. Lévy, H. Berger, P.E. Schmid, Phys. Rev. B 52 (1995) 7771–7774.
[28] C.N.R. Rao, B. Raveau, Transition Metal Oxides, VCH, New York, 1995.
[29] B.G. Hyde, S. Andersson, Inorganic Crystal Structures, Wiley, New York, 1989.
[30] S.J. Clark, M.D. Segall, C.J. Pickard, P.J. Hasnip, M.J. Probert, K. Refson, M.C. Payne, Z. Kristallogr. 220 (2005) 567–570.
[31] J.P. Perdew, K. Burke, M. Ernzerhof, Phys. Rev. Lett. 77 (1996) 3865–3868.
[32] D. Vanderbilt, Phys. Rev. B 41 (1990) 7892–7985.
[33] H.J. Monkhorst, J.D. Pack, Phys. Rev. B 16 (1977) 1748.
[34] P. Villars, L.D. Calvert (Eds.), Pearson's Handbook of Crystallographic Data for Intermetallic Phases, 2nd ed., ASM International Materials Park, OH, 1991.
[35] Ulrich Gesenhues, J. Phys. Chem. Solids 68 (2007) 224–235.
[36] A. Stashans, S. Lunell, R.W. Grimes, J. Phys. Chem. Solids 57 (1996) 1293.
[37] Yanqin Gai, Jingbo Li, Shu-Shen Li, Jian-Bai Xia, Su-Huai Wei, Phys. Rev. Lett. 102 (2009) 036402.
[38] P. Murugan, R.V. Belosludov, H. Mizuseki, T. Nishimatsu, T. Fukumura, M. Kawasaki, Y. Kawazoe, J. Appl. Phys. 99 (2006), 08M105.
[39] J. Sun, H.T. Wang, J.L. He, Y. Tian, J. Phys. Rev. B 71 (2005) 125132.